Ion-beam-induced epitaxial regrowth of amorphous layers in silicon on sapphire

J. Linnros, B. Svensson,* and G. Holmén
Department of Physics, Chalmers University of Technology, S-41296 Göteborg, Sweden
(Received 8 March 1984)

A neon ion beam has been used to regrow epitaxially a ~1700-Å-thick amorphous surface layer in silicon on sapphire at low temperatures. The damaged layer was produced by implanting 80-keV silicon ions to a dose of 2×10^{15} ions/cm^2 at room temperature. The channeling technique with 315-keV protons was used to investigate the depth distribution of the damage, and disorder depth profiles were extracted from the backscattering spectra using calculations based on multiple-scattering theory. The epitaxial regrowth was quantitatively determined from the extracted profiles. Many of the parameters which influence the regrowth rate, such as dose, dose rate, target temperature, energy, and random or channeled direction for the annealing beam, were varied. The results were compared with energy deposition calculations which indicated strongly that the annealing rate depends on the energy deposited in elastic collisions by the annealing ion beam. A defect annealing model based on vacancy diffusion is discussed.

I. INTRODUCTION

Ion implantation of dopants in semiconductor materials has several advantages in comparison with conventional diffusion techniques. Various parameters, such as the depth distribution of the dopants, the dose, and the lateral diffusion, can be controlled much more accurately. However, the energetic ions introduce damage along their tracks which must be removed in an annealing process. The object is to restore the crystal structure and position the dopants on substitutional sites where they can be electrically active. The conventional way of achieving this is by thermal annealing at 500 °C to 1000 °C where ordinary solid-phase epitaxial regrowth occurs. It has also been demonstrated that a high-power laser or electron beam, as well as pulses of such beams, can be used to heat the samples to these temperatures or even higher, where liquid-phase epitaxial regrowth is obtained. This local heating technique can also be accomplished with an intense ion beam.[1,2] Baglin *et al.*[1] used a pulsed 280-keV proton beam to recrystallize an amorphous surface layer with a dose corresponding to ~1 J/cm^2. Unfortunately, the methods where high temperatures are involved eventually cause a broadening of the dopant distribution. Therefore, low-temperature processes would be more profitable for the fabrication of semiconductor devices.

Silicon films on insulating substrates, such as silicon on sapphire (SOS), have aroused great interest due to the possibility of making components with lower capacitance and higher speed. The stacking of such thin silicon films would enable three-dimensional component structures to be fabricated. For these layers a low-temperature annealing method is necessary to prevent dopant diffusion and defect formation which alter their electrical properties.

Recently it has been shown that the annealing of radiation damage in semiconductors can be achieved with the use of an ion beam at a much lower annealing temperature (200—300 °C) than in conventional methods. Holmén *et al.*[3,4] studied radiation damaged layers in germanium with the secondary electron emission method and found that ion-induced annealing occurs at a given dose rate if the target temperature is held above a certain threshold. This critical temperature increases with dose rate and ion mass.

Such an annealing process is also present when damaged layers are formed during ion implantation. For silicon it is well known that the dose required to form an amorphous layer increases with temperature and decreases with ion mass and dose rate.[5–7] For instance, for high fluences of boron implantation at room temperature, Eisen *et al.*[6] found a strong dependence of the amount of disorder produced on dose rate.

For still lighter ions, such as H^+ and He^+, ion-induced annealing has been demonstrated even at room temperature.[7–10] Kool *et al.*[9] reported an annealing effect for carbon implanted silicon bombarded with 200-keV H^+ or He^+ ions. They observed that the damage peak from the C^+ implantation was slightly reduced, whereas at larger depths damage could be introduced by the annealing beam. Furthermore, the initial annealing rate was proportional to the amount of disorder and a lower ion energy was seen to increase the annealing rate.

Epitaxial regrowth of amorphous material due to ion bombardment has been demonstrated, provided that crystalline material is present to act as a seed for the regrowth.[11–15] A sufficiently high energy of the ion beam is also required so that the annealing ions are able to pass through the amorphous/crystalline interface. Golecki *et al.*,[11] for example, used 250-keV Si^+ ions to induce regrowth of a 2300-Å-thick amorphous layer in silicon at 300 °C. However, they observed that disorder was produced at a depth corresponding to the projected range of the annealing ions. Nakata *et al.*[12,13] used a high-energy ion beam, 2.56 MeV As^+, to anneal completely a 650-Å-thick amorphous surface layer in silicon. The target was heated to 290 °C by the ion beam itself. They reported that the recrystallized layer thickness increased linearly with ion dose and substrate temperature.

Ion annealing of a buried amorphous layer in SOS has been performed in a previous experiment[16] using a 300-keV Ne^+ beam. The regrowth proceeded from both sides of the amorphous layer and the number of defects decreased approximately logarithmically with dose in the interval 5×10^{14} to 5×10^{15} ions/cm^2.

In this work a study of the ion-beam-induced epitaxial regrowth of amorphous surface layers in silicon on sapphire is performed using the channeling technique. The amount of damage is extracted from the backscattering spectra by applying disorder depth profile calculations. The purpose is to study systematically the dependence of the rate of regrowth on various parameters such as target temperature, ion dose, dose rate, and ion energy. An effort will be made to explain the results in terms of a mechanism closely related to the energy depositied in nuclear collisions.

II. EXPERIMENT

A. Experimental setup

The target material used was silicon on sapphire (SOS) (Union Carbide). The 1.0-μm-thick intrinsic (100) silicon layer had been grown on a $(1\bar{1}02)$ sapphire substrate by a chemical-vapor-deposition (CVD) method. This film thickness was selected due to its lower backscattering yield compared to thinner silicon layers, indicating a lower damage concentration in the thicker films. The SOS wafers were cut, etched in a dilute HF solution, and rinsed in an ultrasonic bath. They were mounted on a target holder attached to a goniometer which was movable in three orthogonal directions. The target could be rotated around two perpendicular axes lying in the crystal plane and heated to 400 °C by a surrounding oven. Two thermocouples, attached to the target holder, were used to measure the temperature.

The target chamber, shown in Fig. 1, was an ultrahigh-vacuum system, operating at a pressure of 2×10^{-9} Torr, connected to the 400-kV-ion accelerator as well as the 50-kV isotope separator at the Ion Physics Laboratory, Göteborg. The ion-beam current could be measured in a Faraday cup or at the target, where a negatively biased

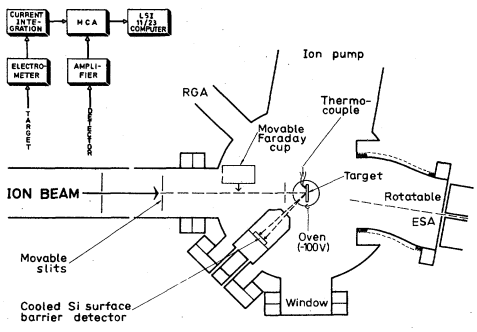

FIG. 1. Experimental setup. MCA represents multichannel analyzer, RGA represents residual gas analyzer, and ESA represents electrostatic analyzer.

shield around the oven acted as an electron suppressor. Current integration electronics were used to achieve high accuracy of the dose measurements.

B. Procedure

The experiments were performed with three different ion beams in four stages, but using the same ultrahigh vacuum (UHV) system under permanent vacuum.

1. Damage production

A 1730-Å-thick amorphous surface layer was created by implantation of 80-keV Si^+ ions to a dose of 2×10^{15} ions/cm^2 at room temperature. The dose rate was below 2×10^{12} ions/cm^{2}s and the target was bombarded in a direction 7° off the ⟨100⟩ axis in order to minimize channeling effects. The critical angle for channeling of the silicon beam in the ⟨100⟩ direction in silicon is, according to Lindhard,[17] of the order of $\psi_2=3.4°$. Each bombarded area, 3 mm^2 in size, was produced with a scanned ion beam to ensure a homogeneous implantation. At first, the isotope $^{29}Si^+$ was used in order to minimize any contamination with impurities, especially N_2^+. However, as the ion current ratios for the different Si isotopes were in accordance with the isotope abundances for Si, the majority of the implantations were performed with $^{28}Si^+$. In addition, the backscattering spectra of the damaged layers were identical within the experimental accuracy for these two isotopes.

2. Channeling analysis

315-keV protons entering in the ⟨100⟩ direction were used for the channeling analysis. The backscattered particles were collected at a scattering angle of 135° with a surface barrier detector which was cooled to −50°C to improve the energy resolution. The proton energy and the geometry used enabled a study of the silicon film down to the sapphire interface with an energy resolution of ~7 keV, corresponding to 450 Å at the surface. For each backscattering spectrum, the total integrated H^+ charge was 2.0 μC probing a 0.5-mm^2 spot in the middle of the implanted area. The beam, with a divergence of less than 0.1°, was aligned with the ⟨100⟩ axis within 0.1° by observing the minimum of the backscattered particles at a nearby unimplanted area. For different implanted spots, the total integrated yield varied less than 3.2%, for unimplanted spots, it varied less than 2.8%, while different measurements on the same spot showed a 0.5% variation. Thus, the variations for different spots were mainly attributed to differences in the silicon film thicknesses and in the damage concentrations of the virgin material rather than inaccuracy of the dose measurements.

3. Ion-beam annealing

The ion-beam annealing procedure was performed with 300-keV $^{20}Ne^+$ ions, bombarding a 3-mm^2-large area along the ⟨100⟩ direction of the SOS samples. According to the Lindhard-Scharff-Schiøtt (LSS) theory[18] the projected range R_p and the straggling for neon ions in amor-

TABLE I. Ranges for experimental parameters for Ne bombardment of 1-μm-thick SOS.

Dose	3×10^{15}–(-2×10^{17} cm^{-2})
Temperature	150–($-$400 °C)
Energy	100–($-$600 keV)
Dose rate	1×10^{13}–(-3×10^{14} cm^{-2}s^{-1})
Direction	⟨100⟩ or 7° off ⟨100⟩

phous silicon is 5600 and 1250 Å, respectively, at 300 keV.[19] These estimations are supported by recent measurements by Grahmann and Kalbitzer[20] for the electronic stopping power of low-energy neon ions in silicon, which showed a good agreement with the LSS theory. Since the neon beam is immediately scattered when passing through the damaged layer, the use of a theory which is valid for amorphous material is justified.

With the use of a scanned ion beam, with scanning frequencies in the interval 0.2–1 kHz, the dose rate was normally kept below 3×10^{13} ions/cm^2 s so that beam heating effects could be eliminated. The influence of dose, temperature, etc., was examined using the values given in Table I. For the highest dose rate (3×10^{14} ions/cm^2 s), the temperature rise of the surface at the center of the beam spot was estimated to be less than 10 °C.[21] During each annealing stage one implanted area was left as a thermal reference to enable the pure thermal annealing at that temperature to be estimated.

4. *Regrowth analysis*

See Sec. II B 2 for the measurement of the damage distributions after annealing.

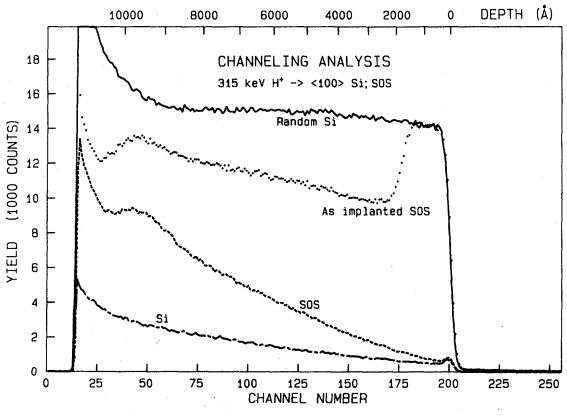

FIG. 2. Backscattering spectra (⟨100⟩, aligned) for unimplanted (100) bulk silicon, (100) silicon on sapphire (SOS), and a SOS sample implanted with 2×10^{15} $^{28}Si^+$ ions/cm^2 (80 keV) at room temperature. A random spectrum for bulk silicon is also shown.

III. RESULTS

In Fig. 2, a random backscattering spectrum for silicon together with spectra from virgin bulk silicon and virgin $\sim$1.0-μm-thick silicon on sapphire are shown. The random spectrum was obtained in the ⟨100⟩ direction after multiple implantations which completely amorphized the crystal to a depth exceeding 1 μm.

For SOS, the yield is higher than for Si. The difference begins with a surface minimum yield of 5% and 3.5%, respectively, increases with depth, and is largest at the silicon/sapphire interface at 10 000 Å. This indicates that defects are present in the SOS material and they have been identified mainly as twins and stacking faults.[22]

A spectrum from SOS implanted with 2×10^{15} ions/cm^2 80-keV $^{28}Si^+$ ions is also shown in Fig. 2 and indicates an amorphous layer extending from the surface to a depth of 1730 Å. The higher yield from 2000 Å and inwards, as compared to the virgin SOS spectrum, is due to dechanneling of the analyzing proton beam in the amorphous surface layer.

Calculations of the depth profile for the energy deposited in elastic collisions of the incoming Si beam were performed using the moments given by Winterbon,[19] in order to estimate theoretically the depth of the amorphous layer. If an average displacement energy of 20 eV per atom is assumed for amorphization at room temperature, the deposited energy should be at least 10^{24} eV/cm^3 or 5 eV/Å for the dose used. Thus, a 1650-Å-thick amorphous layer would be expected.

The depth scale was constructed using a random stopping power for the protons on their outgoing path, taken from Andersen *et al.*[23] and a channeled stopping power on their ingoing path. The ratio of the two stopping powers was taken from Cembali *et al.*[24] For an amorphous layer, this results in an overestimated depth, 12% (1940 Å) for the "as-implanted" spectrum shown in Fig. 2.

A. Dose dependence

Figure 3 shows the dose dependence of the ion-beam annealing. From the spectra it can be seen that the annealing process starts from the amorphous/crystalline interface of the initially damaged surface layer and proceeds epitaxially towards the surface. At the same time the yield at about 6000 Å becomes higher due to damage created approximately at the projected range R_p of the annealing Ne^+ ions. This damage initially increases with dose but saturates at a certain level according to the disorder depth profile calculations (see Fig. 6).

At 200 °C the annealing proceeds slowly with dose and the damaged surface layer is not removed even for a dose of 2×10^{17} ions/cm^2. The deeper introduced damage also protrudes to the surface, largely inhibiting further annealing. At 300 °C the initial annealing rate is almost 5 times higher and a completely regrown layer is obtained after a dose of 1.2×10^{17} ions/cm^2. For this dose, the yield behind the surface minimum yield is only slightly higher than for a virgin crystal but will increase for larger doses. The dose behavior at 400 °C shows an initial annealing

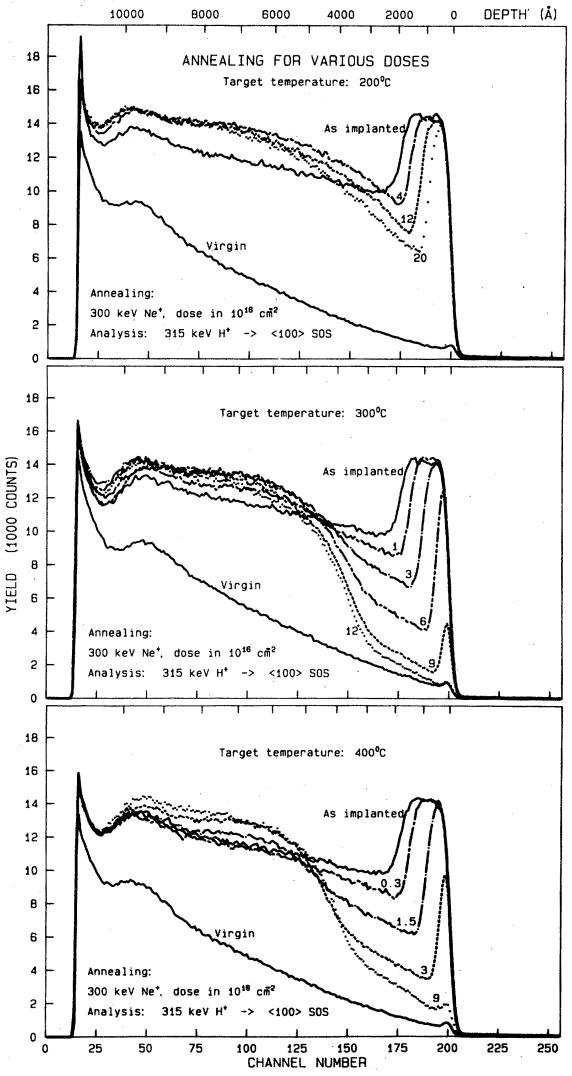

FIG. 3. Backscattering spectra (⟨100⟩, aligned) for SOS samples implanted with 2×10^{15} $^{28}Si^+$ ions/cm^2 (80 keV) and subsequently annealed with various doses of 300-keV $^{20}Ne^+$ ions at 200 °C, 300 °C, and 400 °C, respectively.

rate 3 times higher than that at 300 °C, and for a dose of less than 9×10^{16} ions/cm^2 the damaged layer is regrown. But at 400 °C the surface peak is higher and further bombardment gives an increasing amount of damage.

B. Temperature dependence

Figure 4 shows the dependence on target temperature for annealing with 300-keV $^{20}Ne^+$ ions at a constant dose of 6×10^{16} ions/cm^2. A higher temperature is seen to increase the efficiency of the annealing beam. However, a similar figure with spectra showing the best regrown layers, irrespective of dose, would favor a temperature of ~300 °C. At 150 °C, no annealing occurs and, instead, an amorphous zone which ranges from a depth of ~4000 to ~7000 Å is formed by the implanted neon ions at the dose used.

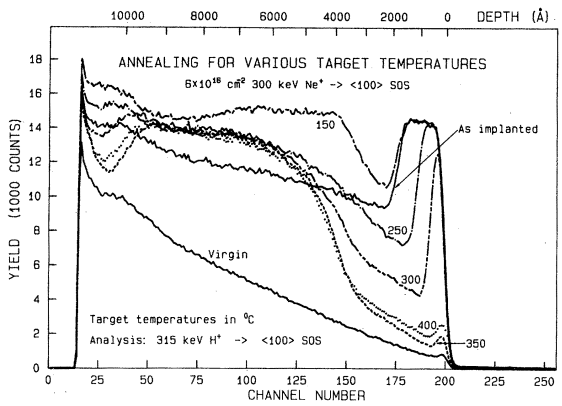

FIG. 4. Backscattering spectra (⟨100⟩, aligned) implanted with 2×10^{15} $^{28}Si^+$ ions/cm^2 (80 keV) and subsequently annealed with 6×10^{16}/cm^2 $^{20}Ne^+$ ions (300-keV) for various target temperatures.

C. Energy Dependence

The results of annealing with different energies at a constant target temperature of 300 °C and a dose of 6×10^{16} ions/cm^2 are presented in Fig. 5. A low-energy ion anneals more effectively. However, the damage created around R_p is deposited closer to the surface, which limits the thickness of the regrown layer.

D. Dependence on other parameters

Annealing with different dose rates, ranging from 1×10^{13} to 3×10^{14} ions/cm^{2}s, to a constant dose of 6×10^{16} ions/cm^2 did not alter the channeling spectra. Only for the highest dose rate was the residual amorphous layer slightly thinner, possibly caused by a small beam heating effect.

In all of the experiments reported above, the annealing beam was aligned with the ⟨100⟩ axis. To estimate the

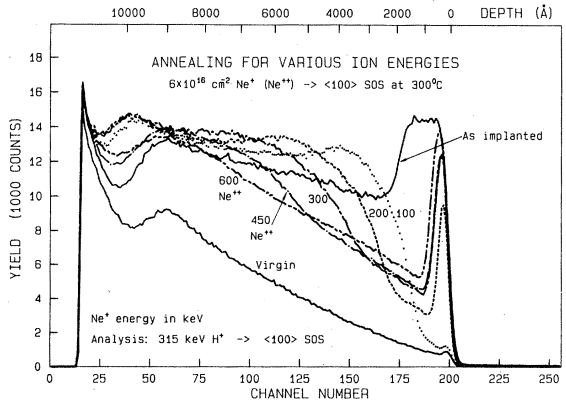

FIG. 5. Backscattering spectra (⟨100⟩, aligned) for SOS samples implanted with 2×10^{15} $^{28}Si^+$ ions/cm^2 (80 keV) and subsequently annealed with 6×10^{16}/cm^2 of $^{20}Ne^+$ or $^{20}Ne^{2+}$ ions at 300 °C for various ion energies.

influence of any channeling effect of the bombarding Ne^+ ions on the annealing, the target was tilted 7° off the ⟨100⟩ axis. For a 300-keV neon beam channeled along the ⟨100⟩ axis in silicon the critical angle is of the order of $\psi_2=2.3°$.[17] The thicknesses of the regrown layers were identical to the ones in Fig. 3, within experimental accuracy. The lack of dependence on random-channeling direction reflects the very fast scattering of the annealing neon beam in an amorphous layer. According to multiple-scattering theory (see Sec. IV A), after traveling a distance of approximately 250 Å, already 50% of the 300-keV neon beam is scattered through an angle greater than the critical angle for channeling.

IV. DEPTH PROFILES OF LATTICE DISORDER

In order to analyze quantitatively the backscattering spectra and extract the dependence of the annealing rate on various parameters, we have used a technique discussed by several authors[25–30] and reviewed by Behrisch and Roth.[31] The propagating ion beam, initially aligned with a low-order crystal axis, is divided into two parts: one channeled and one dechanneled or random part. The channeled component is sensitive to structural defects in the crystal, e.g., point defects, stacking faults, and microtwins. Such defects result in backscattering of the ions or just in minor deflections which tend to dechannel the ions. The dechanneled component encounters all atoms and is backscattered as in amorphous material. This can be summarized by the expression

$$\chi(t)=[1-\chi_D(t)]\frac{N'(t)}{N}+\chi_D(t)\ , \tag{1}$$

where $\chi(t)=y(t)/y_N(t)$ and represents the normalized yield at a depth t, $y(t)$ is the channeled yield from a damaged crystal, $y_N(t)$ is the normal or random yield, $\chi_D(t)$ is the dechanneled fraction of the beam, N is the atomic density equal to 4.978×10^{22} cm^{-3} for Si, and $N'(t)$ is the number of defects at the depth t, to be evaluated.

An approximate expression for the dechanneled fraction of the ion beam is

$$\chi_D(t)=\chi_V(t)+[1-\chi_V(t)]P(t)\ , \tag{2}$$

where $\chi_V(t)=y_V(t)/y_N(t)$ and represents the normalized yield from an undamaged crystal and $P(t)$ is the probability that an ion is deflected more than a critical angle ψ_C due to many small-angle scattering events at the defects, when penetrating from the surface to the depth t.

Equation (2) separates dechanneling due to defects and normal dechanneling, from lattice vibrations for example, somewhat arbitrarily.[26] $P(t)$ is usually calculated with multiple- or plural-scattering theory which is valid for amorphous layers with randomly distributed scattering centers. Thus, the best results are expected for amorphous layers at the surface or embedded in a single crystal.[32] For a damaged crystal which is not amorphous, the channeled and the random components of the ion beam encounter different densities of scattering centers. In such a layer, a multiple-scattering treatment of the dechanneling with a single function for $P(t)$ seems to be less appropriate. The extracted number of defects, or disordered atoms, is somewhat difficult to interpret since different kinds of defects have different scattering cross sections. The defect distribution may also be correlated with the crystal lattice, as for example with vacancies, where it is weighted by the lateral flux distribution of the channeled ions making the assumption of random scattering centers rather crude. However, when the type of defect is known, a specific scattering cross section can be applied[30,33–35] to determine the number of defects.

A. Multiple scattering at defects

$P(t)$ is evaluated using a multiple-scattering distribution derived by Sigmund and Winterbon.[36] Their theory assumes small scattering angles and neglects all energy loss, which implies that the calculations will be most accurate in the first 5000 Å, where the relative energy loss of 315-keV H^+ is less than 10%. The multiple-scattering distribution, $F(t,\alpha)$, is integrated for all angles greater than ψ_c, the critical angle for channeling:

$$P(t)=\int_{>\psi_c}F(t,\alpha)d\Omega=\int_{\tilde{\psi}_c}^{\infty}\tilde{\alpha}f_1(\tau,\tilde{\alpha})d\tilde{\alpha}=P(\tau)\ , \tag{3}$$

where α is the total deflection angle for which the tangent of α is substituted in the small-angle approximation, $d\Omega$ is the solid angle belonging to α and $f_1(\tau,\tilde{\alpha})$ is tabulated in Ref. 36 for $0.001\le\tau\le2000$. The reduced quantities $\tilde{\alpha}$ and τ and the Thomas-Fermi screening radius a are defined as

$$\tilde{\alpha}=\frac{Ea}{2Z_1Z_2e^2}\alpha\ , \tag{4}$$

$$\tau=\pi a^2\int_0^t N'(t')dt'\ , \tag{5}$$

$$a=0.8853a_0(Z_1^{2/3}+Z_2^{2/3})^{-1/2}\ , \tag{6}$$

where E is the ion energy, Z_1,Z_2 are the atomic numbers of the ion and target atoms, respectively, a_0 is the Bohr radius, and e is the elementary charge.

Equation (3) is integrated numerically using the tabulated distribution values which are based on the Thomas-Fermi interaction potential. For $\tau<0.2$, i.e., for a small amount of integrated disorder, a single scattering distribution is used, which is derived from (3) in the small-τ limit:[36]

$$\lim_{\tau\to0}P(\tau)=\int_{\tilde{\psi}_c}^{\infty}\frac{\tau}{\tilde{\alpha}^2}f(\tilde{\alpha})d\tilde{\alpha}\ , \tag{7}$$

where $f(\tilde{\alpha})$ is a function determined by the interaction potential. For the Thomas-Fermi potential the following approximate formula for $f(\tilde{\alpha})$ is used:[37,38]

$$f(\tilde{\alpha})=\lambda\tilde{\alpha}^{1-2m}[1+(2\lambda\tilde{\alpha}^{2-2m})^q]^{-1/q}\ , \tag{8}$$

where $m=0.311$, $\lambda=1.70$, and $q=0.588$.

Solving Eqs. (1) and (2) for $N'(t)$ gives the defect concentration at depth t, but since this quantity also appears in Eq. (5), where it is integrated with the depth scale described above, the calculations are iterative for each depth t and proceed inwards. For the yields $y_V(t)$ and $y_N(t)$, the spectrum shown in Fig. 2 for virgin bulk silicon and the random spectrum, respectively, are used.

B. Critical angle

The critical angle in the high-energy limit is, according to Lindhard,[17] of the order of

$$\psi_1 = \left[\frac{2Z_1 Z_2 e^2}{dE} \right]^{1/2}, \quad (9)$$

where d is the distance between the atoms along the rows parallel to the incident beam. For 315-keV protons channeled along the ⟨100⟩ direction in silicon, $\psi_1 = 0.88°$.

According to Eq. (9), the critical angle should increase with depth due to energy loss. However, in Eq. (4) the reduced angle decreases with depth, reflecting an enlarged scattering cross section. With these effects in mind, together with the great sensitivity of the dechanneling rate on the critical angle, ψ_c is treated as a parameter to be varied. For this purpose, 5×10^{14} ions/cm^2 of 100-keV Ne^+ ions were implanted and analyzed. The disorder depth profiles were calculated from the resulting spectrum, from the spectrum from an implantation of 2×10^{15} ions/cm^2 of 80-keV Si^+ (see Fig. 2), and from spectra from implantation of 1×10^{15}-ions/cm^2 of 300-keV Si^+ ions, both in SOS and bulk silicon.[16] For the true ψ_c the level behind the damaged layer should return to the undamaged SOS level (or bulk silicon level, respectively). The best fit was achieved with $\psi_c = 0.75°$, which was easily established within 3%. $\psi_1 = 0.88°$ divided by the fitted value of ψ_c gives a value of 0.85, which is in agreement with the value given by Picraux.[27]

The depth scale used in Eq. (5) is based on the stopping power for ⟨100⟩ aligned protons. In the case of thick amorphous layers, this results in an increase in τ which gives an excessively high dechanneled component. Therefore, the results would be improved if a depth scale that is dependent on the disorder level could be added to the calculations.

V. RESULTS FROM CALCULATIONS

Figure 6 shows some of the disorder depth profiles, calculated from the backscattering spectra in Fig. 3. To improve the clarity of the figure, the calculated depth profiles have been smoothed with a Gaussian function having a full width at half maximum (FWHM) of four channels. The statistics are good at the surface and at the damaged surface layer, where direct scattering is dominant, but get worse with depth owing to the smaller fraction of channeled ions. The defect density for the implanted sample during the first 1700 Å is very close to the atomic density for Si, indicating a totally amorphous surface layer. Beyond 2500 Å the defect density follows that for virgin SOS. The negative values just before 10 000 Å, where the calculations stop, are due to the silicon/sapphire interface where the yield in the backscattering spectra drops. The disorder profiles confirm the epitaxial regrowth of the amorphous layer with a resulting damage comparable to virgin SOS after an annealing dose of 1.2×10^{17} Ne^+ ions/cm^2.

In Fig. 7 the number of removed defects, that is the number of defects in the initially damaged spectrum minus the number of defects in the annealed spectrum, is

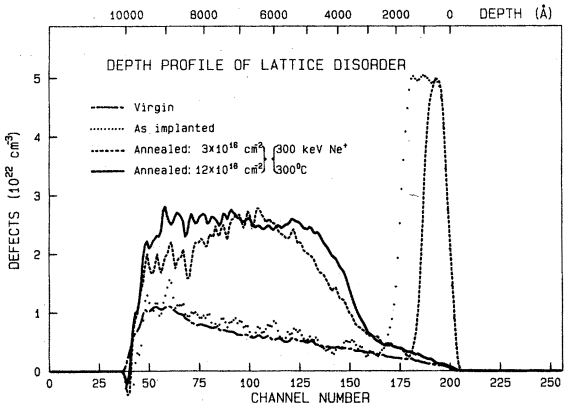

FIG. 6. Depth profiles of lattice disorder for an SOS sample implanted with 2×10^{15} $^{28}Si^+$ ions/cm^2 (80 keV) and subsequently irradiated with various doses of 300-keV $^{20}Ne^+$ ions at 300 °C. A disorder profile for an unimplanted SOS sample is also shown.

shown as a function of the annealing dose for three target temperatures. In this case the number of defects, integrated over the interval 0 to 2500 Å, refers to predominantly amorphous material and consequently the number of annealed defects equals the number of recrystallized atoms. The values at zero dose represent the thermal references which could be viewed as the starting points for the ion annealing. The observed thermal annealing, occurring at the less heavily damaged amorphous/crystalline interface, is less than 10% of the total amount of disorder even if continued for hours at 400 °C. The level where all defects are annealed, which is the same level as for virgin bulk silicon, is shown as well as the level for virgin SOS.

The number of annealed defects increases with dose,

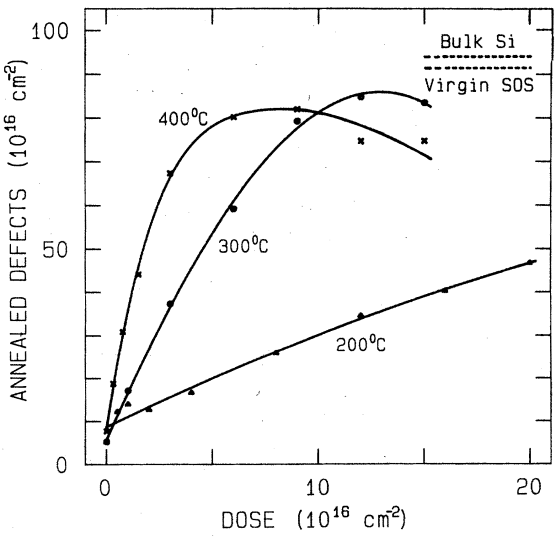

FIG. 7. Number of annealed defects, extracted from the disorder depth profiles by integration in the depth interval 0 to 2500 Å, as a function of the 300-keV Ne^+ ion dose for three different target temperatures.

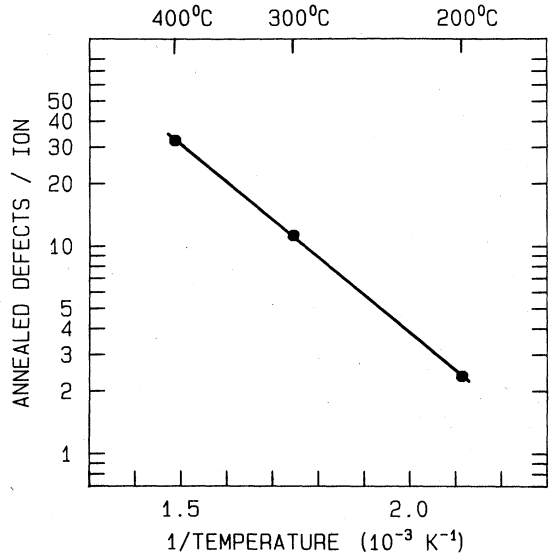

FIG. 8. Initial annealing rate as a function of the reciprocal absolute temperature.

with a higher initial rate for higher temperatures. The best result is, however, reached for 300 °C at a dose of 1.2×10^{17} ions/cm^2. At higher doses the amount of annealed defects decreases with dose, which reflects the fact that the neon disorder profile extends into the integration interval.

A third- or fourth-order polynomial was fitted to the experimental data for each temperature by the method of least squares. These curves are shown in Fig. 7 and the logarithm of the derivative of each polynomial at zero dose is plotted as a function of the reciprocal absolute temperature in Fig. 8. From the resulting Arrhenius plot an activation energy of 0.36 eV can be extracted.

VI. DISCUSSION

A. Factors influencing the ion-beam annealing

The annealing rate of the amorphous surface layer, shown in Fig. 3, is much lower than the annealing rate of a buried amorphous layer in Ref. 16. This is probably due to a difference in the initial amount of damage for the two cases. For the deep implantation of silicon ions the dose was less by a factor of 2, but still created a 4000-Å-thick damaged layer. Thus, the amorphous/crystalline transition region was larger and contained more easily annealed defects. However, at a dose of $\sim10^{16}$ ions/cm^2, when the easily annealed defects have been removed, the annealing rates are comparable. The observed thermal annealing also occurs at the partly damaged amorphous/crystalline transition regions. For the buried amorphous layer approximately 500 Å were regrown at each side of the damaged layer while for the present amorphous surface layer only ~100 Å were thermally regrown. Thus a considerable difference exists in the initial amount of damage for the two implantations. Continued thermal treatment did not result in any further observable regrowth which is consistent with a negligible regrowth rate, ~3 Å/h. This regrowth velocity was derived from thermal annealing data of epitaxial regrowth in the ⟨100⟩ direction of silicon[39] extrapolated to 400 °C.

The yields for the regrown layers have not been reduced below the yields for unimplanted SOS material. Evidently, the original defects in the SOS material, i.e., twins and stacking faults, are stable and are not easily removed. The explanation is probably that when an amorphous layer regrows, these defects grow on the underlying seed of extended defects, and the original amount of damage reappears. In this context it should be emphasized that the theory for the disorder profiles assumed randomly distributed pointlike defects. Extended defects, with different cross sections, were not considered owing to the great difficulty in separating the contributions in an intermixed layer. However, for virgin SOS material, results by Campisano *et al.*[35] indicate that if dechanneling from randomly distributed rows is considered, the number of such rows per cm^3 is a factor of 10 lower than our defect density for virgin SOS in Fig. 6.

The backscattering spectra, as well as the disorder profiles, show that the damage created by the annealing neon beam is centered around ~5500 to 6000 Å. This corresponds approximately to the projected range for 300-keV Ne^+ ions whereas the mean damage depth is ~4000 Å. The same effect has also been reported by several authors[11,40,41] for implantations at elevated temperatures. Furthermore, the disorder depth profile for the sample annealed with 1.2×10^{17} ions/cm^2 at 300 °C resembles the implantation profile for the neon ions. Experiments with the same neon beam to the same dose on a virgin crystal produced a nearly identical spectrum, disregarding a little shift towards increased depth (due to the lower stopping power for the channeled neon ions). These observations suggest that during high dose implantation in silicon at elevated temperatures, some stable disorder is created along the ion-implantation profile. At high temperatures, defects are able to migrate and we speculate that in order to accommodate the high concentration of implanted ions, extended defects are formed which require annealing temperatures of more than 800 °C.[40]

The backscattering spectra in Figs. 3 and 4 for ion annealing at 350 °C and 400 °C show that the amount of damage at the surface of the completely regrown layers is higher than at 300 °C and the damage increases at still higher doses. The same effect also appears at implantations of neon in virgin silicon for doses larger than $\sim3\times10^{16}$ ions/cm^2 at these temperatures. The phenomenon may be related to diffusion of neon atoms towards the surface or to bubble formation[42] occurring at high neon concentrations, but may as well be explained for by defect diffusion which results in extended defects or defect clusters.

The epitaxial regrowth of amorphous layers during thermal annealing depends on the concentration and the kind of impurity introduced during implantation. For a review, see Ref. 43. Low concentrations of *n*- and *p*-type dopants enhance the regrowth rate while other impurities such as rare gases retard the growth. A neon concentration in excess of 1 at. % is known to block the epitaxial recrystallization.[42] In the present experiment, the neon concentration at 2000 Å is $\sim0.4\%$ for a dose of 1×10^{17}

ions/cm^2. Since the regrowth proceeds towards the surface the concentration will be much smaller even for the layers regrown at 200 °C. Therefore, the neon concentration is not believed to be responsible for the decrease in regrowth rate with dose, which can be seen in Fig. 7.

Sputtering of the (amorphous) silicon surface due to the neon bombardment is considered to have only a minor effect on the measurements. According to EerNisse,[44] for 300-keV Ar^+ ions, the sputtering yield is approximately 1.0 atoms/ion, which gives an upper limit for the sputtered layer of $\sim$200 Å at a dose of 10^{17} ions/cm^2. Andersen and Bay[45] found for 45-keV Ne^+ ions on amorphous silicon a sputtering yield of 0.85. Extrapolation to 300 keV using the theory of Sigmund[46] gives an estimated sputtering yield of 0.3, in which case the sputtering effect is negligible compared to the depth resolution of the detector. Nevertheless, the backscattering spectra such as those in Fig. 3 show no evidence of sputtering. This can be inferred from the constant position of the silicon/sapphire interface.

The results show that the annealing was independent of dose rate in the region 1×10^{13} to 3×10^{14} ions/cm^{2}s at 300 °C. In comparison, measurements on germanium[3,4] showed that at a certain temperature a high dose rate produced damage, whereas a low dose rate was able to anneal defects. However, for neon ions on germanium with the dose rates used here, this temperature occurs at $\sim$200 °C. In the present case a dose-rate dependence might therefore be expected in the temperature range where the ion-beam annealing begins (150—200 °C).

B. Ion-beam annealing mechanism

The results shown in Fig. 5, where the annealing ion energy is varied, indicate that the energy deposited in nuclear collisions plays a dominant role in the annealing process. Low-energy ions have a high nuclear energy deposition density in the depth interval of the amorphous layer and the observed annealing rate is high. Annealing with different kinds of ions, having the same energy, also supports this view. Helium ions scarcely induce annealing at all while higher mass ions are more effective.[47] The same argument could also give an explanation for the initial shape of the curves in Fig. 7, where the annealing rates decrease towards the surface presumably as a consequence of the decreasing nuclear energy deposition density.

The importance of the energy deposited in elastic collisions is also supported by other experiments. Kool *et al.*[9] found that a lower energy for the annealing H^+ and He^+ beams was favorable, while having the annealing beam aligned with a crystal axis decreased the annealing rate considerably, possibly due to fewer close collisions for the channeled ions. However, for neon ions we found that the annealing rate was independent of crystal alignment since the amorphous layers almost immediately scattered the ion beam. Further illustration of the role of elastic collisions can be seen in experiments with high-energy electrons which showed that annealing was possible at an energy of 1 MeV but not with 100-keV electrons.[10,48] The effect was attributed to the necessity to have sufficient displacement energy ($>$20 eV in silicon).

The activation energy found, 0.36 eV, is within experimental accuracy, close to the activation energy for the neutral vacancy, 0.33 eV. On the other hand, thermal annealing exhibits an activation energy between 2.35 and 2.85 eV which reflects diffusion in the amorphous region. Nakata *et al.*[12,13] found an activation energy of 0.18 eV which coincides with diffusion of the double-negative vacancy. They concluded that it was created by conversion of the neutral vacancy due to electrons and holes produced by electronic scattering of the energetic ion beam.

Consequently, the following model for the ion-beam annealing mechanism can now be put forward. Because of elastic collisions, the ion beam produces vacancies and interstitials in the crystalline region below the amorphous layer. These point defects are free to migrate and the vacancy diffusion is governed by the observed activation energy. The amorphous/crystalline interface acts as a sink for these vacancies where they recombine either with an atom from the amorphous phase or with an interstitial atom, and as a result they contribute to recrystallization, as indicated in Fig. 9. However, the initially created vacancy could be converted to another kind of defect, e.g., the double-negative vacancy proposed by Nakata *et al.* In such a process, a high electronic stopping of the ion beam might contribute by supplying electrons which may alter the charge state of the created vacancy and increase its mobility. The result would be an enhanced annealing rate but, evidently, the last described process is not necessary for ion-beam annealing to occur. The model relies on a mechanism occurring in the crystalline material below the damaged layer which is given support by, for instance, the extracted activation energy. However, to certify that the ion-beam annealing is not related to processes in the amorphous region some definite proof might be needed.

Since the diffusion of the neutral vacancy appears to be the process which limits the regrowth rates, it is possible to estimate roughly the mean diffusion distance from the interface. At 300 °C the initial regrowth rate is $\sim$11.3 annealed defects per incoming neon ion and the corresponding nuclear energy deposition density is $\sim$7.3 eV/Å at 1730 Å. With an atomic displacement energy of 20 eV for the creation of a vacancy and assuming that only vacancies produced in the vicinity of the interface contri-

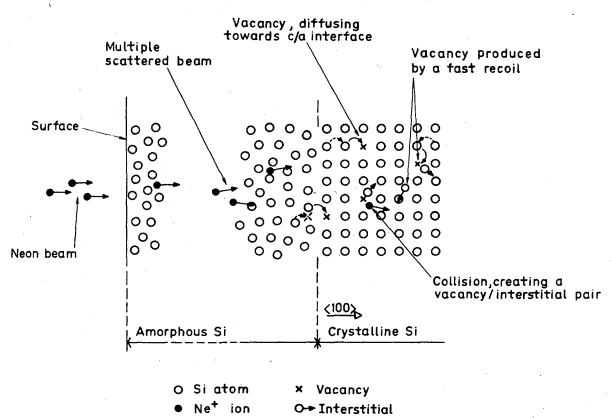

FIG. 9. Schematic view of a model for ion-beam-induced recrystallization.

bute, the distance from which vacancies diffuse would be ~30 Å.

For a damaged layer which is far from amorphous, the ion-beam annealing rate is proportional to the number of defects which can be annealed.[9] In the view of the above model, the vacancies do not migrate to a sink in the form of an interface in this case, but rather diffuse to randomly distributed defects. As a consequence, a different annealing rate would be expected and has been observed for the annealing of the less heavily damaged regions of a buried amorphous layer.[16]

VII. SUMMARY

In conclusion, we have shown that a neon ion beam of a few hundred keV energy can be used to regrow completely a ~2000-Å-thick amorphous layer in silicon provided that the temperature is held above 200 °C. Due to damage created at $\sim R_p$ for the annealing beam, a high energy is preferable while a heavy ion increases the annealing rate. The results favor a model where vacancies and interstitials, created in the crystalline material due to the energy deposited in nuclear collisions by the ion beam, diffuse towards the amorphous/crystalline interface where they contribute to the recrystallization.

ACKNOWLEDGMENTS

The authors thank J. Jacobsson and A. Kangasmaa for skilled technical assistance. Valuable discussions with Anatole Vjatkin, who participated in some parts of the work, were very much appreciated. The work was financially supported by the Swedish Board for Technical Development and the Swedish Natural Science Research Council.

---

*Present address: National Defense Research Institute, Department 3, S-581 11 Linköping, Sweden.

[1]J. E. E. Baglin, R. T. Hodgson, W. K. Chu, J. M. Neri, D. A. Hammer, and L. J. Chen, Nucl. Instrum. Methods **191**, 169 (1981).

[2]G. F. Cembali, P. G. Merli, and F. Zignani, Appl. Phys. Lett. **38**, 808 (1981).

[3]G. Holmén, P. Högberg, and A. Burén, Radiat. Eff. **24**, 39 (1975).

[4]G. Holmén, S. Peterström, A. Burén, and E. Bøgh, Radiat. Eff. **24**, 45 (1975).

[5]J. W. Corbett, J. P. Karins, and T. Y. Tan, Nucl. Instrum. Methods **182&183**, 457 (1981).

[6]F. H. Eisen and B. Welch, Radiat. Eff. **7**, 143 (1971).

[7]E. Bøgh, P. Høgild, and I. Stensgaard, Radiat. Eff. **7**, 115 (1971).

[8]J. K. Hirvonen, W. L. Brown, and P. M. Glotin, in *Proceedings of the Second International Conference on Ion Implantation in Semiconductors, Garmich-Partenkirchen,* edited by I. Ruge and J. Graul (Springer, Berlin, 1971), p. 8.

[9]W. H. Kool, H. E. Roosendaal, L. W. Wiggers, and F. W. Saris, Radiat. Eff. **36**, 41 (1978).

[10]M. D. Matthews and S. J. Ashby, Philos. Mag. **27**, 1313 (1973).

[11]I. Golecki, G. E. Chapman, S. S. Lau, B. Y. Tsaur, and J. W. Mayer, Phys. Lett. **71A**, 267 (1979).

[12]J. Nakata and K. Kajiyama, Appl. Phys. Lett. **40**, 686 (1982).

[13]J. Nakata, M. Takahashi, and K. Kajiyama, Jpn. J. Appl. Phys. **20**, 2211 (1981).

[14]N. N. Gerasimenko, A. V. Dvurechenskii, G. A. Kachurin, N. B. Pridachin, and L. S. Smirnov, Fiz. Tekh. Poluprovodn. **6**, 1834 (1972) [Sov. Phys.—Semicond. **6**, 1588 (1973)].

[15]G. A. Kachurin, Fiz. Tekh. Poluprovodn. **14**, 787 (1980) [Sov. Phys.—Semicond. **14**, 461 (1980)].

[16]B. Svensson, J. Linnros, and G. Holmén, Nucl. Instrum. Methods **209&210**, 755 (1983).

[17]J. Lindhard, Mat. Fys. Medd. Dan. Vid. Selsk. **34**, No. 14 (1965).

[18]J. Lindhard, M. Scharff, and H. E. Schiøtt, Mat. Fys. Medd. Dan. Vid. Selsk. **33**, No. 14 (1963).

[19]K. B. Winterbon, *Ion Implantation Range and Energy Deposition Distributions* (Plenum, New York, 1975), Vol. 2.

[20]H. Grahmann and S. Kalbitzer, Nucl. Instrum. Methods **132**, 119 (1976).

[21]G. Alestig and G. Holmén, J. Appl. Phys. (in press).

[22]W. E. Ham, M. S. Abrahams, C. J. Buiocchi, and J. Blanc, J. Electrochem. Soc. **124**, 634 (1977).

[23]H. H. Andersen and J. F. Ziegler, in *Hydrogen Stopping Powers and Ranges in all Elements,* edited by J. F. Ziegler (Pergamon, New York, 1977), Vol. 3.

[24]F. Cembali and F. Zignani, Radiat. Eff. **31**, 169 (1977).

[25]E. Bøgh, Can. J. Phys. **46**, 653 (1968).

[26]F. H. Eisen, in *Channeling,* edited by D. V. Morgan (Wiley, London, 1973), p. 415.

[27]S. T. Picraux, J. Appl. Phys. **44**, 587 (1973).

[28]J. E. Westmoreland, J. W. Mayer, F. H. Eisen, and B. Welch, Radiat. Eff. **6**, 161 (1970).

[29]L. C. Feldman and J. W. Rodgers, J. Appl. Phys. **41**, 3776 (1970).

[30]S. T. Picraux and P. Rai-Choudhury, in *Characterization Techniques for Semiconductor Materials and Science,* edited by P. A. Barnes and G. A. Rozgonyi, (Electrochemical Society, New Jersey, 1978), p. 447.

[31]R. Behrisch and J. Roth, in *Proceedings of the International Conference on Ion Beam Surface Layer Analysis,* edited by O. Mayer, G. Linker, and F. Käppler (Plenum, New York, 1976), p. 539.

[32]Y. Quéré, Radiat. Eff. **28**, 253 (1976).

[33]G. Foti, L. Csepregi, E. F. Kennedy, J. W. Mayer, P. P. Pronko, and M. D. Rechtin, Philos. Mag. **A37**, 591 (1978).

[34]S. T. Picraux, D. M. Follstaedt, P. Baeri, S. U. Campisano, G. Foti, and E. Rimini, Radiat. Eff. **49**, 75 (1980).

[35]S. U. Campisano, G. Foti, E. Rimini, and S. T. Picraux, Nucl. Instrum. Methods **149**, 371 (1978).

[36]P. Sigmund and K. B. Winterbon, Nucl. Instrum. Methods **119**, 541 (1974).

[37]K. B. Winterbon, P. Sigmund, and J. B. Sanders, Mat. Fys. Medd. Dan. Vid. Selsk. **37**, No. 14 (1970).

[38]K. B. Winterborn, Radiat. Eff. **13**, 215 (1972).

[39]L. Csepregi, E. F. Kennedy, J. W. Mayer, and T. W. Sigmon, J. Appl. Phys. **49**, 3906 (1978).

[40]L. Csepregi, E. F. Kennedy, S. S. Lau, J. W. Mayer, and T. W. Sigmon, Appl. Phys. Lett. **29**, 645 (1976).

[41]J. J. Grob and P. Siffert, Nucl. Instrum. Methods **209&210**,

413 (1983).
[42]M. Wittmer, J. Roth, P. Revesz, and J. W. Mayer, J. Appl. Phys. **49**, 5207 (1978).
[43]J. S. Williams, Nucl. Instrum. Methods **209&210**, 219 (1983).
[44]E. P. EerNisse, J. Appl. Phys. **42**, 480 (1971).
[45]H. H. Andersen and H. L. Bay, J. Appl. Phys. **46**, 1919 (1975).
[46]P. Sigmund, Phys. Rev. **184**, 383 (1969).
[47]G. Holmén, J. Linnros, and B. Svensson, J. Appl. Phys. (in press).
[48]R. S. Nelson, Radiat. Eff. **32**, 19 (1977).